The dust environment of Main-Belt Comet P/2012 T1 (PANSTARRS)

F. Moreno

Instituto de Astrofísica de Andalucía, CSIC, Glorieta de la Astronomía s/n, 18008 Granada, Spain

fernando@iaa.es

A. Cabrera-Lavers

Instituto de Astrofísica de Canarias, c/Vía Láctea s/n, 38200 La Laguna, Tenerife, Spain,

and

Departamento de Astrofísica, Universidad de La Laguna (ULL), E-38205 La Laguna, Tenerife, Spain,

and

GTC Project, E-38205 La Laguna, Tenerife, Spain

O. Vaduvescu

Isaac Newton Group of Telescopes, Apdo. de Correos 321, E-38700 Santa Cruz de la Palma, Canary Islands, Spain

and

Instituto de Astrofísica de Canarias, c/Vía Láctea s/n, 38200 La Laguna, Tenerife, Spain

J. Licandro

Instituto de Astrofísica de Canarias, c/Vía Láctea s/n, 38200 La Laguna, Tenerife, Spain,

and

Departamento de Astrofísica, Universidad de La Laguna (ULL), E-38205 La Laguna, Tenerife, Spain

and

F. Pozuelos

Instituto de Astrofísica de Andalucía, CSIC, Glorieta de la Astronomía s/n, 18008 Granada, Spain

ABSTRACT

Main-Belt Comet P/2012 T1 (PANSTARRS) has been imaged using the 10.4m Gran Telescopio Canarias (GTC) and the 4.2m William Herschel Telescope (WHT) at six epochs in the period from November 2012 to February 2013, with the aim of monitoring its dust environment. The dust tails brightness and morphology are best interpreted in terms of a model of sustained dust emission spanning 4 to 6 months. The total dust mass ejected is estimated at $\sim$6–25$\times10^6$ kg. We assume a time-independent power-law size distribution function, with particles in the micrometer to centimeter size range. Based on the quality of the fits to the isophote fields, an anisotropic emission pattern is favored against an isotropic one, in which the particle ejection is concentrated toward high latitudes ($\pm45^\circ$ to $\pm90^\circ$) in a high obliquity object (I=80°). This seasonally-driven ejection behavior, along with the modeled particle ejection velocities, are in remarkable agreement to those we found for P/2010 R2 (La Sagra) (Moreno et al. 2011a).

Subject headings: minor planets, asteroids: general — comets: individual (P/2012 T1 (PANSTARRS)) — Methods: numerical

1. Introduction

Main-Belt Comet P/2012 T1 (PANSTARRS) was discovered by the Pan-STARRS survey on UT 2012, October 6.53 (Wainscoat et al. 2012). The orbit was identified as that of a Main-Belt Comet (MBC), i.e., an active object in an orbit typical of a main belt asteroid. This object constitutes the 10th identified MBC. The general properties of those objects have been reviewed by e.g. Jewitt (2012). N-body integrations of their orbits reveal that in general they are dynamically stable, with timescales of 100 My or longer (Hsieh et al. 2012), so they seem to be native members of the Main Asteroid Belt (Hsieh et al. 2009). This agrees with the fact that the spectra of some of them can be identified with those of well-known asteroidal families (Licandro et al. 2011), being markedly different to those of bona fide comets. Two objects have been found, however, with shorter lifetimes, namely 238P/Read and P/2008 R1, which were found to be dynamically stable for 20–30 Myr only (Jewitt et al. 2009; Haghighipour 2009), owing to their proximity to the 8:3 and 1:2 mean-motion resonances with Jupiter. Concerning their activity, some of those objects show clearly a sustained activity, of the order of several months, such as P/2010 R2 (La Sagra) (hereafter P/La Sagra) and 2006 VW139 (Moreno et al. 2011a; Licandro et al. 2013), while in some others the activity is restricted to a short time interval, as in the cases of (596) Scheila (e.g., Jewitt et al. 2011; Bing & Hsieh 2011; Moreno et al. 2011b; Ishiguro et al. 2011), and, re-

cently, P/2012 F5 (Gibbs) (Stevenson et al. 2012; Moreno et al. 2012b). The object P/2010 A2 belongs very likely to this latter group (Jewitt et al. 2010; Snodgrass et al. 2010). These authors based their results on a extended dataset, covering various epochs and observation geometries, contradicting our results, based on a more limited dataset, revealing sustained activity (Moreno et al. 2010). In addition, some MBCs have been detected to be recurrent in activity, such as 133P/Elst-Pizarro and 238P (Hsieh et al. 2010, 2011b). Given the small sample of MBCs it is then very important to characterize the emission properties of any new member discovered.

2. Observations and data reduction

CCD images of P/2012 T1 were acquired on several nights from 2012 November 2012, until the end of 2013 February. Table 1 lists the log of the observations. The UT date referred in the table is the mean time of the images acquired at the corresponding night. The labels (a) to (e) are used to facilitate identification of the images in Figures 1-3 and in Table 2. On the WHT, we used the Prime Focus Imaging Platform (PFIP) (Tulloch 1998), the Auxiliary CAMera-spectrograph (ACAM) (Benn et al. 2008), both with a standard Johnson-Cousins R filter, and the Long-slit Intermediate Resolution Infrared Spectrograph (LIRIS) (Manchado et al. 1998), with a K_s filter. On the GTC, we used the Optical System for Image and Low Resolution Integrated Spectroscopy (OSIRIS) camera-spectrograph (Cepa 2010), with a Sloan r' filter. The images were bias and flat field corrected, and calibrated in flux by standard procedures. Each night the object was imaged repeatedly, and a median stack image was obtained by adding-up the available images taking into account the sky motion of the object at the epoch. Figure 1 shows the final images at each night, except on 2013 February 27, in which the object was undetectable. The object looks active at all the other dates, displaying a comet-like tail. On 2013 February 17 the object was already vary faint, with $m_{r'}$=22.9±0.3 and a full-width at half-maximum (FWHM) of 1.8-2″. This is significantly larger than the average seeing on that night, ∼1″, indicating that some circumnuclear dust is still present. However, the noise is considerable, leading to irregularly-shaped isophotes, so that only the measured magnitude will be considered for modeling purposes. We were unable to detect the object on February 27 neither with ACAM nor with LIRIS instruments. Strong moonlight prevented us to detect objects having m_R >18.5 with ACAM. However, with LIRIS K_s band we could detect much fainter objects, allowing us to establish a limiting magnitude for P/2012 T1 of m_{K_s} >22.8±0.1.

For consistency, we converted all the OSIRIS r' magnitudes to the common R standard Johnson-Cousins system by subtracting 0.33 mag, using the transformation equations by

Fukugita et al. (1996), assuming for the object the same spectral dependence as the Sun within the bandpasses of these two red filters (Moreno et al. 2010). Last column in Table 1 lists the geometrically reduced magnitudes of the object calculated by using apertures between 2 and 3 times the FWHM. These magnitudes are given by $m(1,1,0) = m - 2.5\log(\Delta r_h^2) - \phi\alpha$, where m is the apparent magnitude, r_h and Δ are the heliocentric and geocentric distances in AU, ϕ is the phase coefficient, taken as 0.03 mag deg^{-1}, and α is the phase angle. In addition to the images just described, we will use for modeling an early observation by Buzzi (Wainscoat et al. 2012), giving m_R=19.8, or $m_R(1,1,0)$=17.0, on UT 2012 October 11.04.

After flux calibration, the images were rotated to the (N, M) system (Finson & Probstein 1968) through the position angle of the Sun to the target radius vector, and converted to solar disk intensity units (sdu), which are the output units of our Monte Carlo dust tail code.

3. The Model

We applied our Monte Carlo code described previously (e.g., Moreno 2009; Fulle et al. 2010; Moreno et al. 2012a), which computes the trajectory of a large number of particles ejected from a small-sized nucleus, assuming that the grains are affected by the solar gravitation and radiation pressure. The model has many input parameters, and a number of assumptions must be made, as described below. The particle orbital elements are computed from the terminal velocity and the β parameter (e.g. Fulle 1989), which is given by $\beta = C_{pr}Q_{pr}/(2\rho r)$, where C_{pr}=1.19$\times$ 10^{-3} kg m^{-2}, Q_{pr} is the radiation pressure coefficient, and ρ is the particle density, assumed at ρ=1000 kg m^{-3}. The pressure radiation coefficient for absorbing particles with radii $r \gtrsim 1$ μm is $Q_{pr} \sim 1$ (e.g. Moreno et al. 2012a). The particle geometric albedo is assumed at p_v=0.04 (i.e., a Halley-like value).

The main inputs of the model are the ejection velocity law, the size distribution function, and the dust mass loss rate. Of course, all these parameters can be time-dependent. Notwithstanding this, and in order to limit the amount of free parameters, we only allowed the dust loss rate to be time-dependent. A power-law function was assumed for the size distribution of the particles, ejected with a terminal velocity of $v(\beta) = v_0\beta^\gamma$, where v_0 and γ are constants. This expression is commonly accepted for the terminal velocities of grains dragged out from ice sublimation on the surface of cometary nuclei, and also for fragments ejected from collision experiments (e.g., Giblin 1998; Onose & Fujiwara 2004). Then, the onset time (t_0), the ejection velocity parameters, the power-law size distribution index, the limiting sizes of the particles (r_{min},r_{max}), and the dust loss rate (dM/dt) are the free pa-

rameters of the model. We will work under the hypotheses of both isotropic and anisotropic particle ejection scenarios.

Based on the evolution of the dust tail brightness and morphology, we hypothesized a sustained activity pattern for P/2012 T1. The early observation by Buzzi on 2012 October 11.04 (Wainscoat et al. 2012) gives $m_R(1,1,0)$=17.0, while on November 13.1 we estimate $m_R(1,1,0)$=16.9±0.2 (Table 1). Thus, the observed magnitudes are essentially the same in these two dates. If an impulsive event had taken place, in principle we should have noticed a significant magnitude increase in that month period, a logical consequence of having less and less dust particles inside the field of view as they travel away from the nucleus. The magnitude would only be constant in the very unlikely scenario where all particles ejected were slow-moving and large-sized, being essentially unaffected by radiation pressure. But even if that were the case, then the dust tails in the 2012 December and 2013 January images would be depleted of particles in the anti-sunward direction (upper part of the images in Figures 2c and 2d), and would have the wrong orientation. This has been confirmed by test models, and occurs because the synchrones older than those corresponding to discovery date (∼25 days post-perihelion) point to directions away from the anti-solar direction, which is populated mostly by dust particles ejected significantly later.

4. Results and Discussion

In order to find the best fit parameters, we start from our previous experience in the analysis of MBC dust tails, specifically on those for which sustained activity has been derived, as P/La Sagra and 2006 VW139 (Moreno et al. 2011a; Licandro et al. 2013). In those cases, the parameter γ of the ejection velocity was set to γ=1/2, a value which is typical of hydrodynamical drag from sublimating ices and that will be adopted here as well. For the limiting particle sizes, we used a broad range between 5 μm and 1 cm, being distributed following a power-law of index –3.5, the same parameters derived for P/La Sagra. Then, we tried to fit the other parameters, namely t_0, v_0, and the dM/dt profile, in the assumption of isotropic ejection as a first approximation.

For a given date, the fitting quality to the observed images is measured by the quantity $\sigma = \sqrt{\sum (I_{obs} - I_{fit})^2/N}$, where I_{obs} and I_{fit} are the observed and fitted images, the sum being limited to all the observed image pixels N whose brightness is higher than a certain threshold. This threshold is given by the outermost contours of the observed images displayed in Figures 2 and 3. This eliminates from the evaluation of σ the regions of high noise, low brightness levels, that can contribute spuriously to that quantity. The σ parameters at each date are defined as σ_a to σ_d (see Table 2), corresponding to images (a) to (d) of Table 1,

respectively.

Figure 2 displays the fits to the observed isophotes when the onset of activity is set at perihelion time, v_0=25 m s^{-1}, and the dust loss rate profile is that given at the lower rightmost panel of Figure 2 (solid line). We call this model ISO-1. The corresponding synthetic magnitudes on 2012/11/10 and 2013/02/17 are displayed in Table 2. The apertures used to obtain the synthetic magnitudes and their uncertainties on 2013/02/17 are the same as for the real image on that date. We used the same aperture sizes to estimate the magnitude of the synthetic image on 2012/11/10. Thus, as shown in Figure 2 and Table 2, this ISO-1 model provides a good agreement with all the available observations. The lower magnitude limit of m_{K_s} >22.8±0.1 on 2013/02/27 essentially confirms the decrease in brightness predicted by the model: the dust loss rate decays to zero ∼125 days after perihelion, so that the activity lasted about four months. The total ejected mass for this model is 5.8×10^6 kg.

Within the isotropic ejection scenario, we searched for other model parameters that can produce fits of approximately the same quality as those displayed in Figure 2. Thus, for example, the onset time can be displaced backward in time, provided a rearrangement is made in the dM/dt profile just derived for model ISO-1. Then, similar quality fits are obtained by setting the activation date back up to 50 days before perihelion (see also Table 2), if dM/dt is set as shown in Figure 3, dashed line (model ISO-2). In this case, the activity progresses more gently after onset time, instead of the impulsive character of the dM/dt profile of model ISO-1. In this case, M_t=7.8×10^6 kg, the object being active for five months and a half. If the activation date is set even earlier than the mentioned 50 days before perihelion, then there start to appear fitting problems mainly in the 2012 December 13 and 2013 January 17 images, specifically by an excess brightness in the sunward direction. We can then state that P/2012 T1 has been active for a maximum period of about six months.

Regarding the ejection velocities we have no constraints on that parameter. We have not even estimates on size and density of the body that could help at least to estimate the escape velocity. On the other hand, the combination v_0=25 m s^{-1} and γ=1/2 agrees remarkably well with what we found for P/La Sagra, for which we obtained v_0 values ranging from 15.8 to 31.7 m s^{-1} for γ=1/2. Thus, although it is possible to find other solutions modifying both v_0 and γ, we have not attempted such combinations.

The particle size range affects significantly the model results only if r_{max} is varied. The minimum size has only a minor effect provided it is decreased down to 0.5 μm. However, if the maximum size is increased up to 10 cm, the dust mass loss rate profile must be increased in an overall factor of ∼3, respect to that shown in Figure 2, in order to maintain a similar quality fit to the data. In Table 2, the corresponding range of M_t for r_{max}=1–10 cm is shown.

Even considering that the isotropic ejection scenario provides already a reasonable fit to the data, it is interesting to search for possible model solutions regarding anisotropic ejection patterns. The reason is that for P/La Sagra we found a remarkable improvement of the fits for anisotropic ejection coming from a rotating spherical nucleus with high obliquity (I=90°), i.e. the rotation axis located on the orbital plane, and oriented approximately toward the Sun at the time of maximum activity, mimicked the observed isophote field quite accurately. Also, interestingly, this kind of seasonal activity has also been clearly found for 176P for which an orbital obliquity of ∼60° was derived (Hsieh et al. 2011b), although it cannot be neither confirmed nor rejected for the case of 133P (Hsieh et al. 2010).

Thus, we run the model starting from the parameters obtained for ISO-2 model, but for a single active area located between two latitude circles on a spherical nucleus with rotational parameters I (obliquity) and Φ (argument of the subsolar meridian at perihelion). We limited the search to values of I ∼90°, with an active area close to the south polar region. The choice of the south or the north polar region is arbitrary, as the sense of rotation cannot be determined with this model, and the solution that is valid for a given pole orientation is automatically valid for the opposite pole orientation as well. We only set the south polar region to allow a direct comparison with P/La Sagra. The rotation period was set to 3 hours, which could be appropriate for a small asteroid, but it does not influence the results provided it is much shorter than the ejecta age. Our best fit to the data corresponds to rotational parameters set to I=80°, Φ=260°, the active are being located southward of –45° (see Figure 3). This anisotropic ejection model (called ANIS-1) also required changes with respect to the ISO-2 model in both the parameter v_0, that must be increased to v_0=40 m s^{-1}, and in the dM/dt profile, which is very close to that of model ISO-2 (see Figure 2, lower rightmost panel). The total mass ejected for the anisotropic model is obviously near that of ISO-2 model, with a value of 7.5×10^6 kg for r_{max}=1 cm. As can be seen from Figure 3 and the σ values of Table 2, the overall agreement with the observations for this model is better than for isotropic models. Considering the lower rightmost panels of Figures 2 and 3, the maximum ejection rate occurs approximately 30 days post-perihelion, corresponding to a subsolar point latitude of ∼–80°. We have also tried to fit the observations with the ejection parameters of ISO-1 model (i.e., starting activity suddenly at perihelion), but the results were poorer.

The significance of results of the anisotropic model is that, in a remarkably similar way to MBCs P/La Sagra and 176P, the ejection pattern of P/2012 T1 is compatible with emission from a single high latitude region of a nucleus whose rotation axis is near the orbital plane. Also the latitudes of the subsolar point at perihelion (where the outgassing is nearly maximum) are similar (–60° for P/La Sagra and –70° for P/2012 T1). This is important regarding the numerical calculations by Samarasinha (Samarasinha et al. 2004,

and references therein) which indicate that when a dominant active region is present on a comet the rotational angular momentum vector of the spin state evolves toward the orbital direction of the peak outgassing (or the opposite to it), owing to minimum torque reasons. It would then be interesting to see whether this ejection pattern appears again in subsequent perihelion passages and if other MBCs could be interpreted the same way.

5. Conclusions

The Monte Carlo dust tail model applied to images of P/2012 T1 acquired at La Palma WHT and GTC telescopes allowed us to infer the following conclusions:

1) Taking into account the time evolution of the brightness and morphology of the observed tails, we infer that the ejection of dust from P/2012 T1 has been likely sustained in time, and not produced by an impulsive event. As a result of the modeling we infer that the activity lasted a period of ∼4–6 months, with a total ejected dust mass of order 6–25×10^6 kg, for maximum particle sizes of r_{max}=1–10 cm.

2) The activity pattern could be compatible with that produced by grains being dragged out from the asteroid surface by sublimating ices. However, the nature of the mechanism(s) triggering and maintaining the activity is unknown. The onset of the activity could have been occurred either suddenly near perihelion time, or could have been triggered about a month earlier, and progressing more gradually. We favor this second scenario.

3) The best fits to the data occur for anisotropic ejection scenarios, where the activity takes place mostly from high latitude locations on a nucleus whose rotating axis is nearly contained on the orbital plane and pointing close to the perihelion point. This scenario is remarkably consistent to that found for P/La Sagra, and agree with the seasonally-driven behavior also found for 176P (Hsieh et al. 2011a). If this behavior is confirmed at future perihelion passages or found on other MBCs, it would then have important consequences regarding their nature and evolutionary path. To date, however, the current MBCs database is still small as to establish any firm conclusion.

This article is based on observations made with the Gran Telescopio Canarias (GTC), installed in the Spanish Observatorio del Roque de los Muchachos of the Instituto de Astrofísica de Canarias, in the island of La Palma, and on observations made with the William Herschel Telescope (WHT) operated on the island of La Palma by the Isaac Newton Group in the Spanish Observatorio del Roque de los Muchachos of the Instituto de Astrofísica de Canarias.

We are indebted to Pedro J. Gutiérrez for fruitful discussions. This work was supported by contracts AYA2011-30613-C02-01, AYA2012-39691-C02-01 and FQM-4555 (Junta de Andalucía). J. Licandro gratefully acknowledges support from the Spanish "Ministerio de Ciencia e Innovación" projects AYA2011-29489-C03-02 and AYA2012-39115-C03-03.

REFERENCES

Benn, C., Dee, K., & Agócs, T. 2008, Ground-based and Airborne Instrumentation for Astronomy II. Edited by McLean, Ian S.; Casali, Mark M., Proc. SPIE, 7014, 70146X-1

Bing, Y., & Hsieh, H.H., 2011, ApJ, 737, L39

Cepa, J. 2010, Highlights of Spanish Astrophysics V, Astrophysics and Space Science Proceedings, Springer-Verlag, p. 15

Finson, M., & Probstein, R. 1968, ApJ, 154, 327

Fukugita, M., Ichikawa, T., Gunn, J. E., et al. 1996, AJ, 111, 1748

Fulle, M., 1989, A&A, 217, 283

Fulle, M., Colangeli, L., Agarwal, J., et al. 2010, A&A, 522, 63

Giblin, I. 1998, Planet. Space Sci., 46, 921

Haghighipour, N. 2009, Meteoritics & Planet. Sci., 44, 1863

Hsieh, H.H., & Jewitt, D., & Ishiguro, M. 2009, AJ, 137, 157

Hsieh, H.H., & Jewitt, D., Lacerda, P., et al. 2010, MNRAS, 403, 363

Hsieh, H.H., Ishiguro, M., Lacerda, P., & Jewitt, D. 2011a, AJ, 142 29

Hsieh, H.H., Meech, K., & Pittichova, J. 2011b, ApJ, 736, L18

Hsieh, H.H., Yang, B., & Haghighipour, N. 2012, ApJ, 744, 9

Ishiguro, M., Hanayama, H., Hasegawa, S. et al. 2011, ApJ, 740, L11

Jewitt, D., Yang, B., & Haghighipour, N. 2009 AJ, 137, 4313

Jewitt, D., Weaver, H., Agarwal, J., et al. 2010, Nature, 467, 817

Jewitt, D., Weaver, H., Mutchler, M., et al. 2011 ApJ, 733, L4

Jewitt, D. 2012 AJ, 143, 21

Licandro, J., Campins, H., Tozzi, G.P., et al. 2011 A&A 532, 65

Licandro, J., de León, J., Moreno, F., et al. 2013 A&A 550, A17

Manchado, A., Fuentes, F.J., Prada, F. et al. 1998, Proc. SPIE, 3354, 448

Moreno, F. 2009, ApJS, 183, 33

Moreno, F., Licandro, J., Tozzi, G.-P., et al. 2010, ApJ, 718, L132

Moreno, F., Lara, L.M., Licandro, J., et al. 2011a, ApJ, 738 L16

Moreno, F., Licandro, J., Ortiz, J.L., et al. 2011b, ApJ, 738, 130

Moreno, F., Pozuelos, F., Aceituno, F., et al. 2012a, ApJ, 752, 136

Moreno, F., Licandro, J., & Cabrera-Lavers, A. 2012b, ApJ, 761, L12

Onose, N., & Fujiwara, A. 2004, Meteoritics and Planet. Sci., 39, 321

Samarasinha, N.H., Mueller, B.E.A., Belton, M. J. S., & Jorda, L. 2004, in Comets II, M. C. Festou, H. U. Keller, and H. A. Weaver (eds.), University of Arizona Press, Tucson, 745 pp., p.281-299

Snodgrass, C., Tubiana, C., Vincent, J.-B. et al. 2010, Nature, 467, 814

Stevenson, R., Kramer, E.A., Bauer, J.M. et al. 2012, ApJ, 759, 142

Tulloch, S., 1998, ING Technical Note 119

Wainscoat, R., Hsieh, H., Denneau, L. at al. 2012 Central Bureau Electronic Telegrams 3252, 1

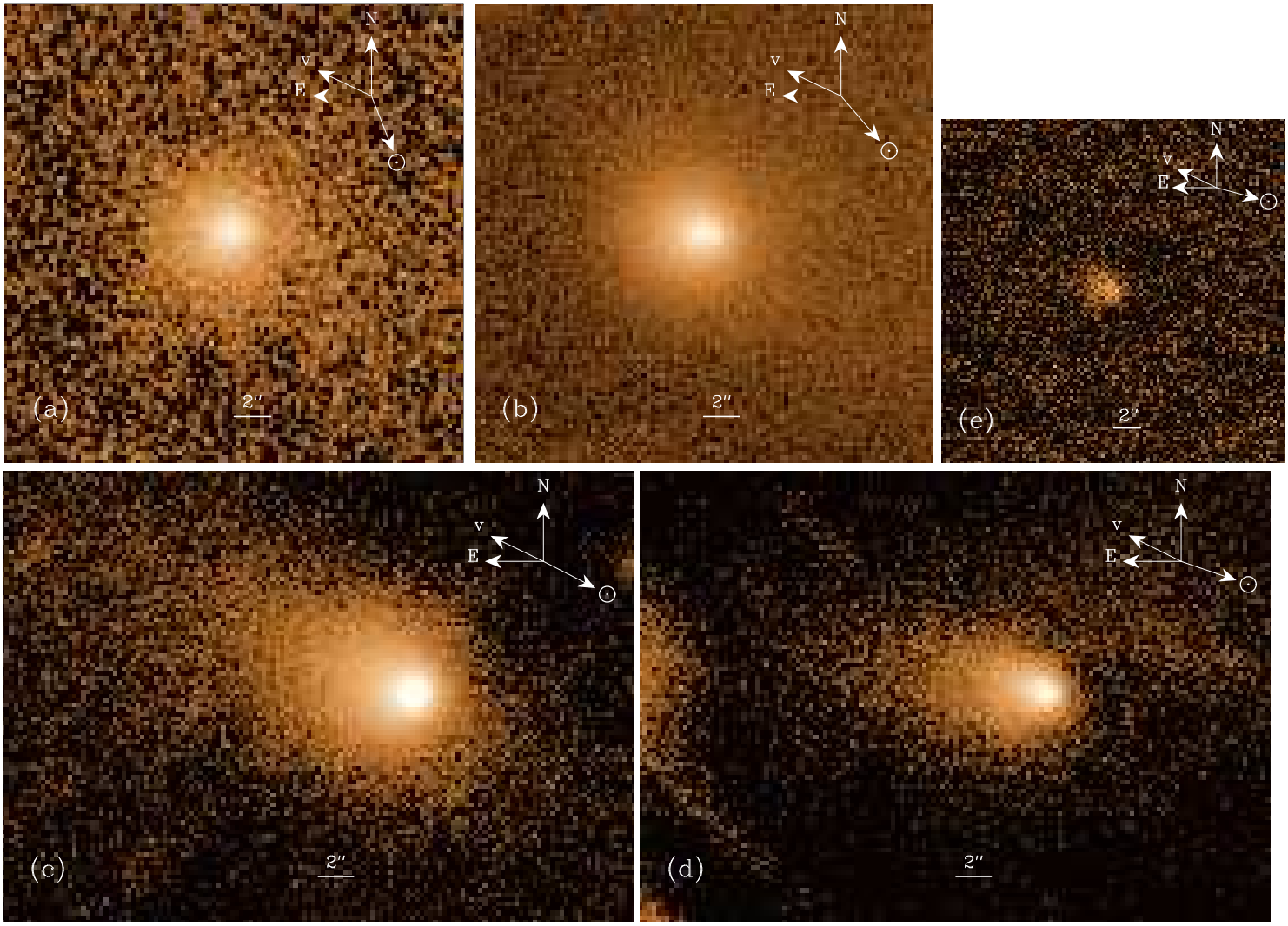

Fig. 1.— Median stack images of P/2012 T1 obtained with PFIP on the 4.2m William Herschel Telescope (a), and OSIRIS on the 10.4m Gran Telescopio Canarias (b-e). The corresponding dates are displayed in Table 1. The directions of the velocity vector, the Sun, and the astronomical North and East are indicated.

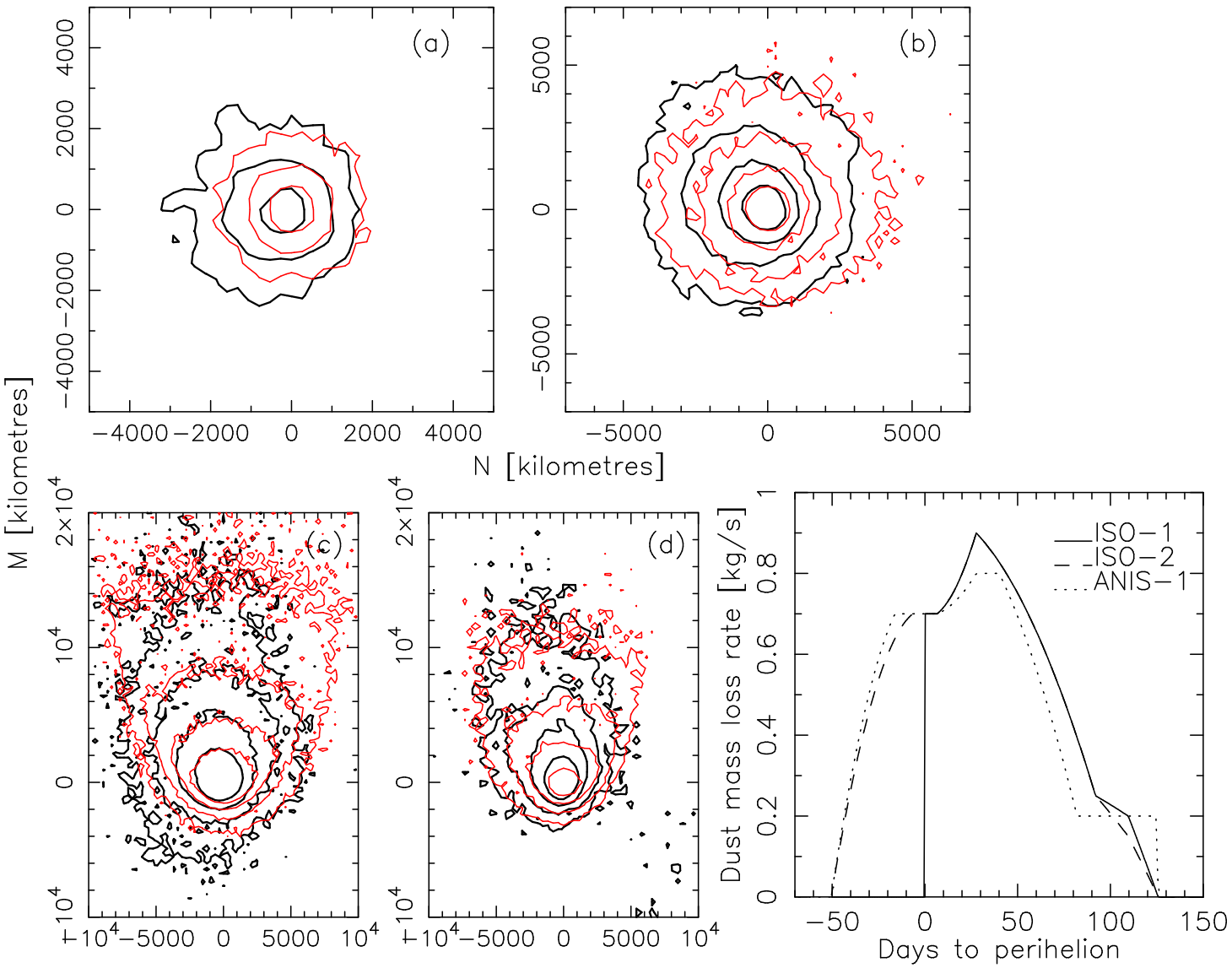

Fig. 2.— Isotropic model with MBC activation at perihelion time (ISO-1 model). Panels (a) to (d) correspond to the observations at the dates indicated in Table 1. The black thick solid lines at panels (a) to (d) indicate the observed isophotes, while the red thin lines correspond to the model. The innermost isophote level in each panel (all expressed in *sdu*) are: (a) 8×10^{-14}; (b) 5.6×10^{-14}; (c) 1.2×10^{-14} ; (d) 1.2×10^{-14}. The isophotes vary in factor of 2 between consecutive levels. The lower rightmost panel displays the dust mass loss rate as a function of time to perihelion, for three models: ISO-1, ISO-2, and ANIS-1 (see text for a detailed description of the models).

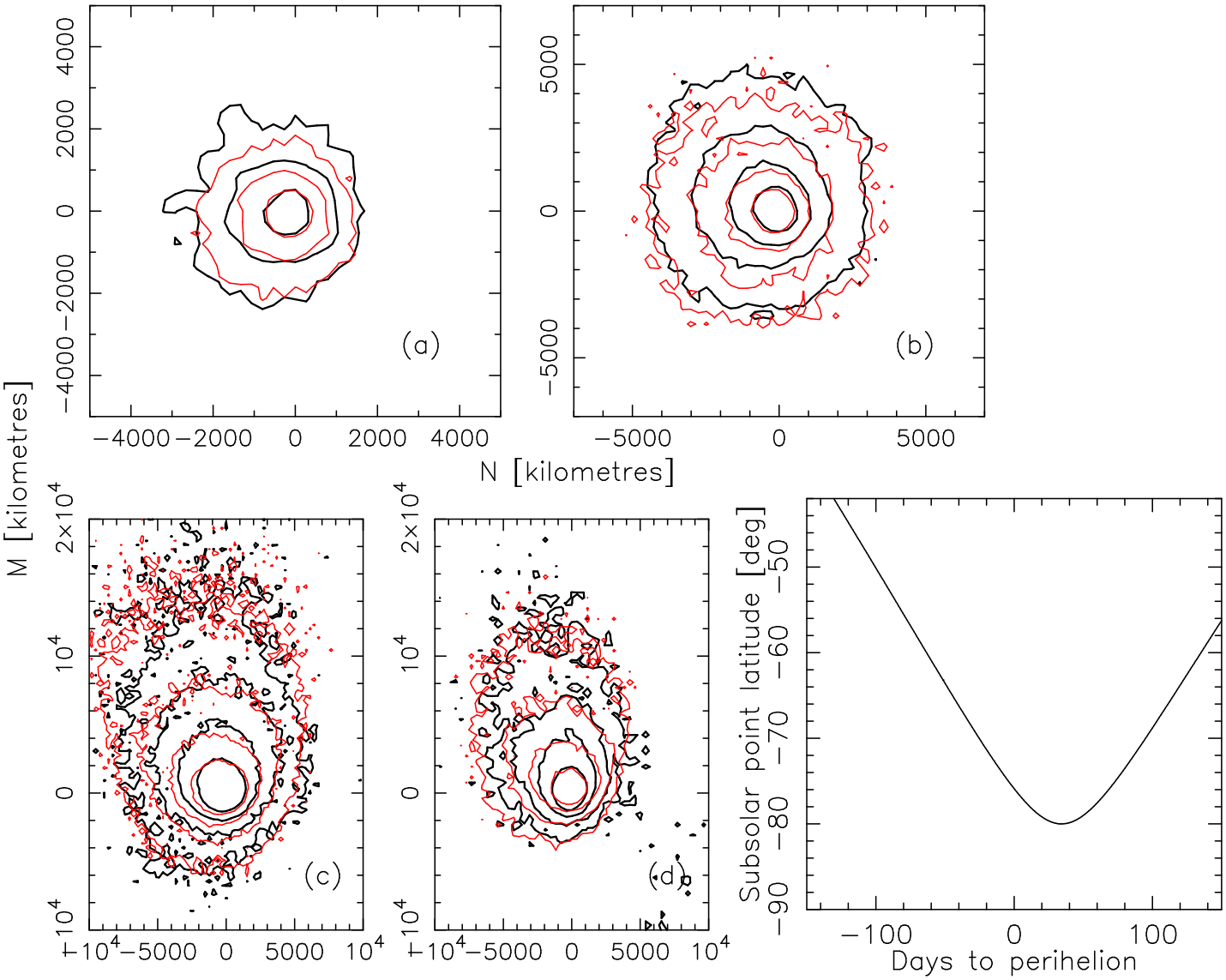

Fig. 3.— Anisotropic model with MBC activation at 50 days before perihelion time (ANIS-1 model). Panels (a) to (d) correspond to the observations at the dates indicated in Table 1. The black thick solid lines at panels (a) to (d) indicate the observed isophotes, while the red thin lines correspond to the model. The innermost isophote level in each panel (all expressed in *sdu*) are: (a) 8×10^{-14}; (b) 5.6×10^{-14}; (c) 1.2×10^{-14} ; (d) 1.2×10^{-14}. The isophotes vary in factor of 2 between consecutive levels. The lower rightmost panel displays the latitude of the subsolar point as a function of time to perihelion.

Table 1. Log of the observations

Date (UT) (id)	Instrument/Telescope	T_{exp}(s)×N_{im} [a]	r_h(AU)	Δ(AU)	α(°)	Resolution (km px^{-1})	$m(1,1,0)$ [b]
2012 Nov 13.10 (a)	PFIP/WHT	20×14	2.43	1.47	6.2	265.8	16.9±0.2
2012 Nov 19.98 (b)	OSIRIS/GTC	60×20	2.44	1.49	8.4	274.8	17.0±0.2
2012 Dec 13.87 (c)	OSIRIS/GTC	60×15	2.46	1.67	16.5	307.1	17.3±0.2
2013 Jan 17.94 (d)	OSIRIS/GTC	60×30	2.51	2.09	22.5	385.4	17.7±0.2
2013 Feb 17.90 (e)	OSIRIS/GTC	20×61	2.55	2.53	22.4	466.4	18.9±0.3
2013 Feb 27.90	LIRIS/WHT	44×60	2.57	2.67	21.7	485.0	>22.8±0.1
2013 Feb 27.93	ACAM/WHT	31×60	2.57	2.68	21.6	485.0	–

[a]Individual exposure time and number of images secured

[b]Geometrically reduced magnitude in R-band except that of LIRIS/WHT that refers to K_s-band apparent magnitude

Table 2. Parameters and results of the models

	MODEL ISO-1	MODEL ISO-2	MODEL ANIS-1	Measured
v_0 (m s^{-1}),γ	125, 1/2	125, 1/2	200, 1/2	
M$_t$ (kg)	6-20$\times10^6$	8-25$\times10^6$	8-25$\times10^6$	
t_0	Perihelion time	–50d to perihelion	–50d to perihelion	
Event duration	125 days	175 days	175 days	
r_{min}	$\leq$5 μm	$\leq$5 μm	$\leq$5 μm	
r_{max}	1–10 cm	1–10 cm	1–10 cm	
Power index	–3.5	–3.5	–3.5	
Rotational I, Φ	–	–	80°, 260°	
Active area	–	–	$[\pm45°, \pm90°]$	
σ_a,σ_b (sdu)	3.8×10^{-14},1.7×10^{-14}	3.7×10^{-14},1.8×10^{-14}	3.1×10^{-14},1.3×10^{-14}	
σ_c,σ_d (sdu)	4.2×10^{-15},1.8×10^{-15}	4.4×10^{-15},1.9×10^{-15}	2.8×10^{-15},1.2×10^{-15}	
m$_R$(2012/10/11)	19.5±0.2	19.4±0.2	19.4±0.3	19.8[a]
m$_R$(2013/02/17)	22.6±0.4	22.5±0.4	22.7±0.4	22.6±0.3

[a]Reported R-mag by Buzzi (Wainscoat et al. 2012)